

## PREPARATION AND CHARACTERIZATION OF Fe<sub>3</sub>O<sub>4</sub>/SiO<sub>2</sub>/TiO<sub>2</sub> COMPOSITE FOR METHYLENE BLUE REMOVAL IN WATER

Adel Fisli<sup>1\*</sup>, Ridwan<sup>1</sup>, Yuni K. Krisnandi<sup>2</sup>, Jarnuzi Gunlazuardi<sup>2</sup>

<sup>1</sup>*Center for Science and Technology of Advanced Materials, National Nuclear Energy Agency, Kawasan Puspiptek, Serpong 15314, Indonesia*

<sup>2</sup>*Department of Chemistry, Faculty of Mathematic and Natural Science, Universitas Indonesia, Kampus UI Depok, Depok 16424, Indonesia*

(Received: January 2016 / Revised: November 2016 / Accepted: January 2017)

### ABSTRACT

The main problem with the slurry process is the difficulty in recovering the photocatalyst nanoparticle from water following purification. An alternative solution proposed the photocatalyst be immobilized on magnetic carriers, which would allow them to be recollected from the water suspension following treatment using an external magnetic field. Magnetically photocatalyst composites were prepared using simple heteroagglomeration by applying attractive electrostatic forces between the nanoparticles with an opposite surface charge. The Fe<sub>3</sub>O<sub>4</sub>/SiO<sub>2</sub>/TiO<sub>2</sub> photocatalysts were synthesized in an aqueous slurry solution containing Fe<sub>3</sub>O<sub>4</sub>/SiO<sub>2</sub> and TiO<sub>2</sub> nanoparticles under pH 5 conditions. Meanwhile, Fe<sub>3</sub>O<sub>4</sub>/SiO<sub>2</sub> was prepared by a simple procedure via a coprecipitation of iron(II) and iron(III) ion mixtures in ammonium hydroxide and was leached by sodium silicate. The synthesized samples were investigated to determine the phase structure, the magnetic properties, and the morphology of the composites by X-ray diffraction (XRD), vibrating sample magnetometer (VSM), and transmission electron microscopy (TEM), respectively. The results indicated that the composites contained anatase and rutile phases and exhibited a superparamagnetic behavior. Fe<sub>3</sub>O<sub>4</sub>/SiO<sub>2</sub> particles, which were of the aggregation spherical form at 20 nm in size, were successfully attached onto the TiO<sub>2</sub> surface. The catalytic activity of Fe<sub>3</sub>O<sub>4</sub>/SiO<sub>2</sub>/TiO<sub>2</sub> composites was evaluated for the degradation of methylene blue under ultraviolet (UV) irradiation. The presence of SiO<sub>2</sub> as a barrier between Fe<sub>3</sub>O<sub>4</sub> and TiO<sub>2</sub> is not only improves the photocatalytic properties but also provides the ability to adsorb the properties on the composite. The Fe<sub>3</sub>O<sub>4</sub>/SiO<sub>2</sub>/TiO<sub>2</sub> (50% containing TiO<sub>2</sub> in composite) were able to eliminate 87.3% of methylene blue in water through the adsorption and photocatalytic processes. This result is slightly below pure TiO<sub>2</sub>, which is able to degrade 96% of methylene blue. The resulting Fe<sub>3</sub>O<sub>4</sub>/SiO<sub>2</sub>/TiO<sub>2</sub> composite exhibited an excellent ability to remove dye from water and it is easily recollected using a magnetic bar from the water. Therefore, they have high potency as an efficient and simple implementation for the dye effluent decolorization of textile waste in slurry reactor processes.

**Keywords:** Composites; Magnetic photocatalysts; Methylene blue

### 1. INTRODUCTION

A nanocatalyst can be isolated or separated from liquid using magnetically separable nanoparticles (Polshettiwar et al., 2011). The magnetically supported catalysts are highly

---

\*Corresponding author's email: adel@batan.go.id, Tel. +62-21-7560922, Fax. +62-21-7560926  
Permalink/DOI: <https://doi.org/10.14716/ijtech.v8i1.2888>

convenient for removing catalyst nanoparticles from water using an external magnetic field without the need for a filtration or centrifugation step in the heterogeneous system, and they can be subsequently reused in another cycle (Jiang et al., 2010). The incorporation of magnetic iron oxide into TiO<sub>2</sub> nanoparticles as the photocatalyst for environmental application has been actively developed (He et al., 2008; Tyrpekl et al., 2011). However, the direct contact of two semiconductors between magnetic iron oxide and TiO<sub>2</sub> gives rise to an unfortunate heterojunction, resulting in an increase in electron-hole recombination and photodissolution, which can lead to a weakening of its photocatalytic activity (Alvarez et al., 2010). Therefore, a barrier layer is necessary to prevent direct contact between iron oxide and TiO<sub>2</sub>. Silica is most commonly used as the barrier layer between iron oxide. Wang et al. (2012) used tetraethyl orthosilicate (TEOS) as silica layer sources and further used tetrabutyl orthotitanate (TBOT) as titanium sources, obtained from the core-shell-shell structure Fe<sub>3</sub>O<sub>4</sub>/SiO<sub>2</sub>/TiO<sub>2</sub>. To reach the anatase phase of TiO<sub>2</sub>, the composites need to be calcined at a temperature above 400°C. Unfavorably, it might change the iron oxide phase from magnetite (Fe<sub>3</sub>O<sub>4</sub>) to hematite ( $\gamma$ -Fe<sub>2</sub>O<sub>3</sub>), which could cause a decrease in the magnetic properties of composites (Bhongsuwan et al., 2013) or an unwanted high-temperature chemical reaction between the materials (Makovec et al., 2011).

Heteroagglomeration is the aggregation of dissimilar particles in the ceramic application, the formation of aggregates by cohesion between particles of different materials. Heteroagglomeration may result in permanent contact via interactions between the electrostatic forces of two particles that differ in charge (Islam et al., 1995; Fisli et al., 2013). The isoelectric point (IEP) of TiO<sub>2</sub> is approximately 6.2 (Suttiponparnit et al., 2011), while the isoelectric point of Fe<sub>3</sub>O<sub>4</sub>/SiO<sub>2</sub> is about 3 (Fisli et al., 2014). The on range 3 < pH < 6.2 of the solution, Fe<sub>3</sub>O<sub>4</sub>/SiO<sub>2</sub> possesses a positive surface charge, whereas TiO<sub>2</sub> has a negative one, so the interactions between electrostatic forces would adhere two particles together. In a previous study, Fe<sub>3</sub>O<sub>4</sub>/SiO<sub>2</sub>/TiO<sub>2</sub> had been prepared by the mechanochemical method using high-energy milling (HEM) (Winataputra et al., 2015). Thus, this study is focused on the preparation of Fe<sub>3</sub>O<sub>4</sub>/SiO<sub>2</sub>/TiO<sub>2</sub> composites through simply adjusting the pH to find different isoelectrostatic point values of an aqueous slurry solution containing Fe<sub>3</sub>O<sub>4</sub>/SiO<sub>2</sub> and TiO<sub>2</sub> nanoparticles and treated with the ultrasonication processes of the mixture. The prepared magnetically separable photocatalyst composites was characterized by various techniques and examined for the removal of dye in water.

## 2. EXPERIMENTAL METHOD

### 2.1. Preparation of Fe<sub>3</sub>O<sub>4</sub>/SiO<sub>2</sub>/TiO<sub>2</sub>

Fe<sub>3</sub>O<sub>4</sub> nanoparticles were prepared by the coprecipitation method, where 5.2 g of FeCl<sub>3</sub>.6H<sub>2</sub>O (Merck) and 2 g of FeCl<sub>2</sub>.4H<sub>2</sub>O (Merck) (mol ratio of Fe(III):Fe(II) = 2:1) were dissolved in 10.3 mL of 1 N HCl and subsequently diluted to 25 mL with deionized water under vigorous stirring. The prepared iron salt solution was dropped into 250 mL of 1.5 M ammonium hydroxide solution under vigorous stirring. A drop-wise 3.2 mL of sodium silicate (27 wt% SiO<sub>2</sub>, Aldrich) was added to the formed black iron precipitate. Subsequently, the pH of the solution was adjusted to less than 10 with the addition of 2 M HCl. The mixture was stirred vigorously for 4 h and left overnight. The black precipitate was separated from the liquid using a magnetic bar and washed with de-ionized water repeatedly until neutral. In another beaker, 4.64 g of TiO<sub>2</sub> (Aldrich) was dispersed into 100 mL of 0.02 M (NH<sub>4</sub>)<sub>2</sub>SO<sub>4</sub> and then sonicated for 30 min at room temperature. The dispersed TiO<sub>2</sub> was mixed into the Fe<sub>3</sub>O<sub>4</sub>/SiO<sub>2</sub> suspension. Subsequently, the pH value of the mixture was adjusted to 5 with the addition of 1 M HCl. The mixture was sonicated for 30 min at room temperature using an ultrasonic processor (VCX model Sonics Vibra Cell) and centrifuged at 4,000 rpm. The solid was dried in the oven at 60°C

overnight, and this continued with another drying at 100°C for 3 h. Finally, the obtained solid was grounded by agate mortar.

## 2.2. Characterization

X-ray diffraction (XRD) patterns were obtained using an X-Ray diffractometer (XD-610 Phillips) at room temperature. The X-ray source was Cu-K $\alpha$  radiation ( $\lambda = 0.154$  nm) in the  $2\theta$  range from 10° to 80°. The average crystallite size was calculated using Scherrer's equation. The rutile and anatase phase compositions (the content of the crystalline region) were determined by calculating the anatase peak-to-rutile peak ratio. The morphology and microstructure of the samples were observed using transmission electron microscopy (TEM). The specimen for TEM investigation was prepared by dissolving a few samples in ethanol and sonicating for 10 sec. The suspension of the sample was deposited on a copper-grid-supported, perforated, transparent, carbon foil. TEM analyses were performed using JEM-1400, JEOL. The magnetic properties of the samples were measured using a vibrating sample magnetometer (VSM) Oxford type 1.2 T at room temperature in a magnetic field range from -1 to 1 tesla.

## 2.3. Evaluation of the Photocatalytic Activity

The photocatalytic activity of the synthesized materials was evaluated in terms of the removal of methylene blue solution from water using a slurry reactor. Approximately 250 mg of the tested materials was dispersed into 250 mL of 20 mg/L methylene blue. The suspension was stirred under a non-UV and UV lamp (2×18 Watts) having a main radiation of 254 nm at room temperature. No pure oxygen was supplied because it has enough oxygen for oxidation photodegradation due to the continuous stirring in atmosphere. The concentration of the methylene blue solution in water was determined using the Lamda 25 Parkin Elmer UV/Vis Spectrophotometer at the wavelength of 661 nm and at a certain time interval.

# 3. RESULTS AND DISCUSSION

## 3.1. Characterization Results

The phase and crystal structure of the prepared sample were determined by X-ray powder diffraction, as illustrated in Figure 1. The diffractogram of prepared Fe<sub>3</sub>O<sub>4</sub> is similar to the standard diffraction pattern of magnetite (JCPDS file no. 03-0863), which has dominant peaks at  $2\theta$  of about 30.2, 35.6, 43.3, 56.8, and 62.7°. Thus, the particles can be indexed to the pure phase of the Fe<sub>3</sub>O<sub>4</sub> structure. The diffraction pattern of the Fe<sub>3</sub>O<sub>4</sub>/SiO<sub>2</sub> curve (SiO<sub>2</sub> coated Fe<sub>3</sub>O<sub>4</sub>) is identical to that of Fe<sub>3</sub>O<sub>4</sub> (uncoated Fe<sub>3</sub>O<sub>4</sub>). This indicates the SiO<sub>2</sub> coating is in an amorphous form. It also shows that diffraction pattern of magnetite in SiO<sub>2</sub> coating Fe<sub>3</sub>O<sub>4</sub> is clearer than that in uncoated Fe<sub>3</sub>O<sub>4</sub>. It shows the stability of the crystalline phase of Fe<sub>3</sub>O<sub>4</sub> nanoparticles after silica coating (Emadi et al., 2013). TiO<sub>2</sub> revealed the occurrence of the anatase phase (JCPDF file no. 21-1272) and rutile phase (JCPDF file no. 21-1276), which have dominant peaks at  $2\theta$  of about 25.28, 36.95, 37.80, 38.57, 48.05, 53.89, 55.06, 62.69, and 27.45 and 36.08, 39.19, 41.22, 44.05, 54.32, 56.64, and 69.08, respectively.

The compositions of the anatase and rutile phases in TiO<sub>2</sub> are determined by analyzing the ratio of the anatase peak (101) at  $2\theta = 25.3^\circ$  to the rutile peak (101) at  $2\theta = 27.4^\circ$  using a slightly modified formula proposed by Hanaor et al. (2012).

$$X_R(\%) = \frac{1}{1 + 0.8 \frac{I_A}{I_R}} \times 100\% \quad (1)$$

$$X_A(\%) = 100 - X_R \quad (2)$$

where  $X_A$  and  $X_R$  are the percentage fractions of rutile and anatase in powder, and  $I_A$  and  $I_R$  are the X-ray intensities of the anatase and rutile peaks, respectively. The  $\text{TiO}_2$  powder was composed of 55% anatase and 45% rutile. The  $\text{TiO}_2$  and  $\text{Fe}_3\text{O}_4/\text{SiO}_2$  mixture results in the  $\text{Fe}_3\text{O}_4/\text{SiO}_2/\text{TiO}_2$  composite in which the magnetite, anatase, and rutile peaks were still clearly observed. This indicates its phase was retained in the composites. Meanwhile, the crystallite size of the  $\text{TiO}_2$  particles was determined from the major diffraction peak (101) plane broadening of the anatase and rutile phases using the well-known Scherrer's formula (Calderon et al., 2015):

$$\text{Crystallite Size} = \frac{0.9\lambda}{B \cos \theta} \quad (3)$$

where  $\lambda$  is the X-ray wavelength,  $\theta$  is the angle of Bragg diffraction, and  $B$  is the difference between the full-width at half maximums (FWHMs) of the peaks. High-purity silicon powder was used as an internal standard to account for the instrumental line broadening effect during crystal estimation. The calculated crystallite size value of nanocrystalline  $\text{TiO}_2$  is found to be about 60 nm and 83.27 nm for anatase and rutile, respectively.

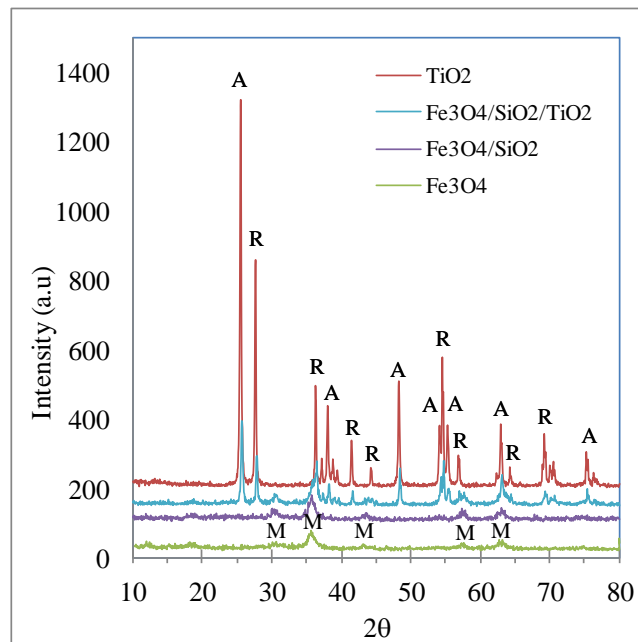


Figure 1 The XRD pattern of the prepared sample (R= rutile, A = anatase, M = magnetite)

The magnetic properties of the prepared sample were measured at room temperature, as illustrated in Figure 2. All samples show the low value of remanent and coercivity magnetization, which indicates that composites showed superparamagnetic behavior. The saturation magnetization values ( $M_s$ ) of each sample are 57.7 emu/gr, 41.1 emu/gr and 29.8 emu/gr for  $\text{Fe}_3\text{O}_4$ ,  $\text{Fe}_3\text{O}_4/\text{SiO}_2$  and  $\text{Fe}_3\text{O}_4/\text{SiO}_2/\text{TiO}_2$ , respectively. The magnetic saturation value of  $\text{Fe}_3\text{O}_4$  is the highest due to it containing pure magnetic and then it decreases following  $\text{Fe}_3\text{O}_4/\text{SiO}_2$  and  $\text{Fe}_3\text{O}_4/\text{SiO}_2/\text{TiO}_2$ , respectively. This is normally due to the non-magnetic phase ( $\text{SiO}_2$  and  $\text{TiO}_2$ ) content increase in the composites. However, all samples are still enough to facilitate the recovery of a photocatalyst composite from treated water by collection using a magnetic bar.

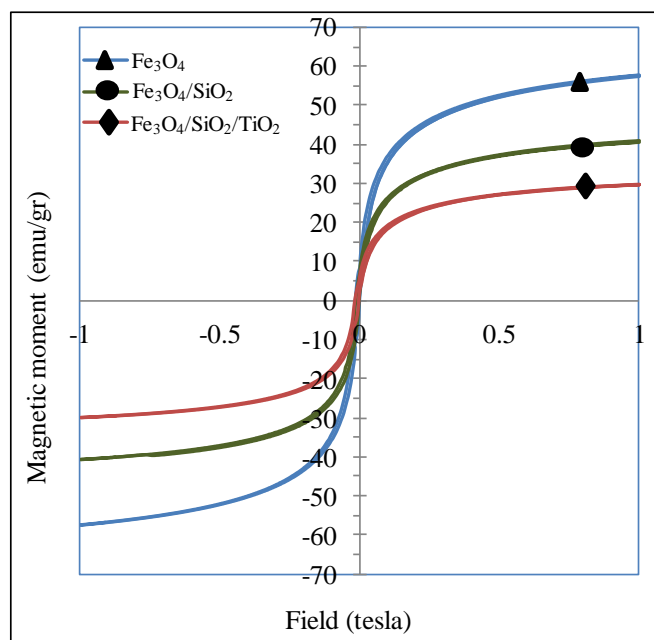


Figure 2 Magnetic hysteresis for the synthesized sample

Figure 3 shows the morphology and microstructure of the resultant samples, which were investigated by TEM. It was expected that  $\text{Fe}_3\text{O}_4$  would be coated by the  $\text{SiO}_2$  layer to form aggregated spherical particles around 20 nm in size. We suspect a large number of  $\text{Fe}_3\text{O}_4$  nanoparticles (dark solid) are encapsulated in the  $\text{SiO}_2$  layer (bright layer) (Figure 3a), which may be responsible for this observation. These color differences arise because of differing electron penetrability. In contrast to the morphology of  $\text{Fe}_3\text{O}_4/\text{SiO}_2$  nanoparticles, Figure 3b clearly shows that the aggregated  $\text{Fe}_3\text{O}_4/\text{SiO}_2$  particles attached successfully onto the  $\text{TiO}_2$  surface. The morphology of the formed aggregate is dependent on the relative particle size. When there is a large difference in particle size, the smaller particles ( $\text{Fe}_3\text{O}_4/\text{SiO}_2$ ) will attach onto the surface of the larger species ( $\text{TiO}_2$ ), which was clearly seen when the  $\text{TiO}_2$  particle size was estimated at around 100 nm in accordance with the manufacturer's recommendations.

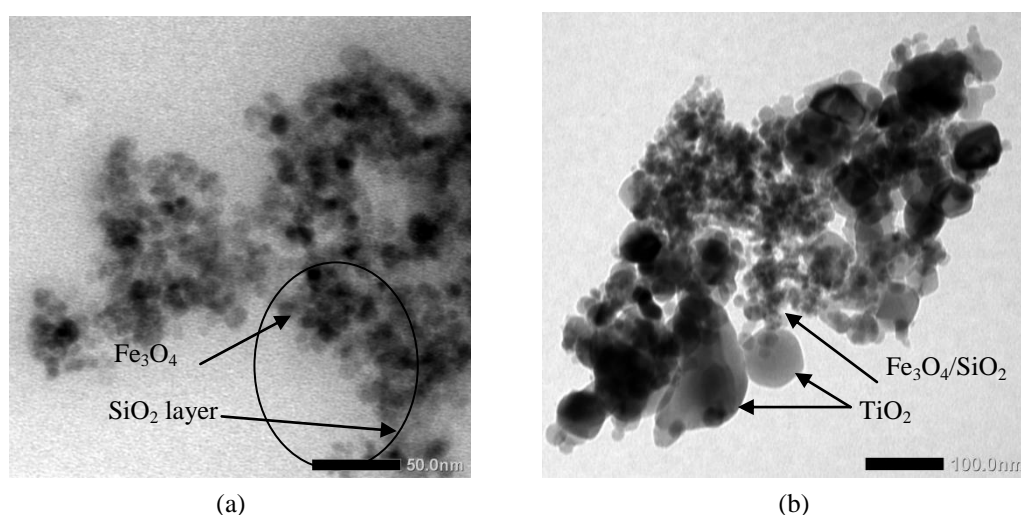


Figure 3 TEM images of (a)  $\text{Fe}_3\text{O}_4/\text{SiO}_2$  and (b)  $\text{Fe}_3\text{O}_4/\text{SiO}_2/\text{TiO}_2$

Magnetic separation is a highly pleasant way to remove and reuse a magnetic photocatalyst from liquid. The magnetism of  $\text{Fe}_3\text{O}_4/\text{SiO}_2/\text{TiO}_2$  composites is exhibited in Figure 4.

$\text{Fe}_3\text{O}_4/\text{SiO}_2/\text{TiO}_2$  is dispersed in water to form a stable suspension for a long time (Figure 4a). If the magnetic bar was dipped into the suspension, the brown particles could be attracted to the magnetic bar and the  $\text{Fe}_3\text{O}_4/\text{SiO}_2/\text{TiO}_2$  photocatalyst could attach completely in less than 5 min, leaving a clear solution (Figure 4b). The  $\text{Fe}_3\text{O}_4/\text{SiO}_2/\text{TiO}_2$  particles plastered on the magnetic bar can be easily removed from the water by lifting the magnetic bar to the top of the container (Figure 4c), so the spent catalysts can be easily reused.

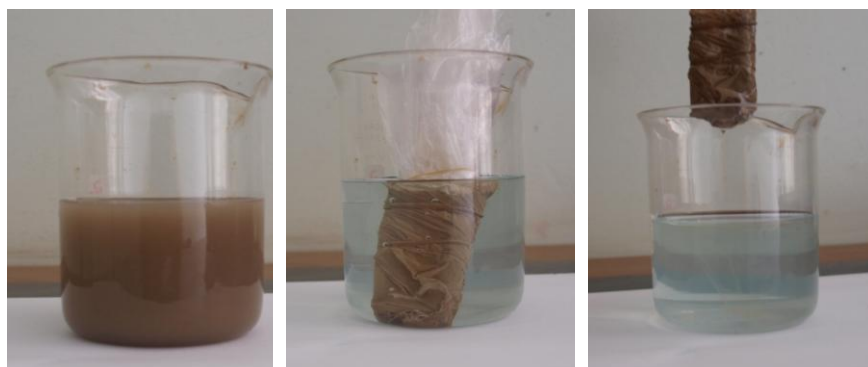


Figure 4 The photographs of the  $\text{Fe}_3\text{O}_4/\text{SiO}_2/\text{TiO}_2$  composite separated from water by applying a magnetic bar

### 3.2. Adsorption Performance

The adsorption performance of the prepared sample was examined to eliminate methylene blue under non-UV irradiation (dark), as shown in Figure 5. The methylene blue concentration in the solution was not eliminated in the presence of both  $\text{TiO}_2$  and  $\text{Fe}_3\text{O}_4/\text{TiO}_2$ , but it can be eliminated significantly in the presence of both  $\text{Fe}_3\text{O}_4/\text{SiO}_2$  and  $\text{Fe}_3\text{O}_4/\text{SiO}_2/\text{TiO}_2$ .

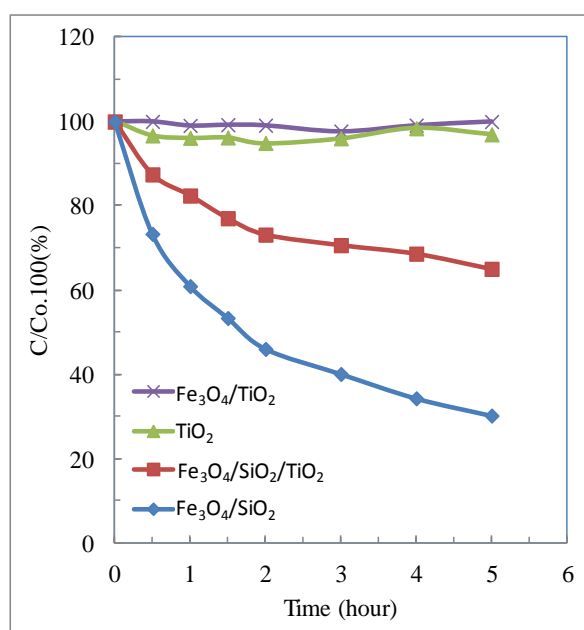


Figure 5 Elimination test of methylene blue under non-UV irradiation (dark)

This result indicates that the adsorption process did not occur for  $\text{TiO}_2$  and  $\text{Fe}_3\text{O}_4/\text{TiO}_2$ , but it occurred for  $\text{Fe}_3\text{O}_4/\text{SiO}_2$  and  $\text{Fe}_3\text{O}_4/\text{SiO}_2/\text{TiO}_2$ . It shows that the presence of  $\text{SiO}_2$  in composites obviously plays a key role in the adsorption process.  $\text{SiO}_2$  is known as an inorganic adsorbent. The surface of  $\text{SiO}_2$  contained silanol (OH group), which can act as the centers of molecular

adsorption during their specific interaction with adsorbates (Zhuravlev, 2000). The adsorption capacity of  $\text{Fe}_3\text{O}_4/\text{SiO}_2$  was higher than that of  $\text{Fe}_3\text{O}_4/\text{SiO}_2/\text{TiO}_2$ . It was reasonable due to the greater fraction of  $\text{SiO}_2$  in  $\text{Fe}_3\text{O}_4/\text{SiO}_2$  than in  $\text{Fe}_3\text{O}_4/\text{SiO}_2/\text{TiO}_2$ , which was 33% versus 16.7%  $\text{SiO}_2$  in  $\text{Fe}_3\text{O}_4/\text{SiO}_2$  and  $\text{Fe}_3\text{O}_4/\text{SiO}_2/\text{TiO}_2$ , respectively.

### 3.3. Photocatalytic Performance

The photocatalytic performance of the prepared sample was examined for the elimination of methylene blue under UV irradiation, as shown in Figure 6. The methylene blue concentration was not eliminated in the presence of  $\text{Fe}_3\text{O}_4$ . On the other hand, as was expected,  $\text{Fe}_3\text{O}_4/\text{TiO}_2$  showed a photocatalytic ability to eliminate 44.2% of the methylene blue concentration during a 5-h process. However, its photocatalytic activity was lower compared to pure  $\text{TiO}_2$ , which was able to eliminate over 96% of the methylene blue concentration over the same period. The low activity of  $\text{Fe}_3\text{O}_4/\text{TiO}_2$  is caused by the low fraction of active  $\text{TiO}_2$  in the composite, and this may be due to the photodissolution effect, which can impair the photocatalytic activity of  $\text{TiO}_2$ . The  $\text{Fe}_3\text{O}_4/\text{SiO}_2/\text{TiO}_2$  composite is able to eliminate 87.3% (12.7% left) of the methylene blue concentration during a 5-h process using the adsorption and photocatalytic processes.  $\text{SiO}_2$  and  $\text{TiO}_2$  played roles at the adsorption and photocatalytic sites, respectively. This is certainly more profitable because more methylene blue can be eliminated. The adsorption process eliminated 35% of methylene blue and the photocatalytic process eliminated 52.3%. The photocatalytic activity of the composite increased from 44.2% ( $\text{Fe}_3\text{O}_4/\text{TiO}_2$ ) to 52.3% ( $\text{Fe}_3\text{O}_4/\text{SiO}_2/\text{TiO}_2$ ). This is due to the photodissolution effect of  $\text{Fe}_3\text{O}_4$ , which decreased on the composites. Thus, this result indicates the function of the presence of  $\text{SiO}_2$  in the composite was not only to prevent the photodissolution effect but also to adsorb methylene blue in water. In the case of photocatalytic activity, the  $\text{Fe}_3\text{O}_4/\text{SiO}_2/\text{TiO}_2$  composite was able to degrade 52.3% of methylene blue, which is lower than that of pure  $\text{TiO}_2$ , which reaches about 96%. When viewed from active containing, the photocatalytic activity of both materials was comparable at 50%  $\text{TiO}_2$  in  $\text{Fe}_3\text{O}_4/\text{SiO}_2/\text{TiO}_2$  and 100%  $\text{TiO}_2$  in pure  $\text{TiO}_2$ . It was reasonable that the photocatalytic activity of  $\text{Fe}_3\text{O}_4/\text{SiO}_2/\text{TiO}_2$  was lower than half that of pure  $\text{TiO}_2$ . The result indicated the photocatalytic activity of  $\text{TiO}_2$  did not decrease, even though it had been composited with  $\text{Fe}_3\text{O}_4$  and  $\text{SiO}_2$ .

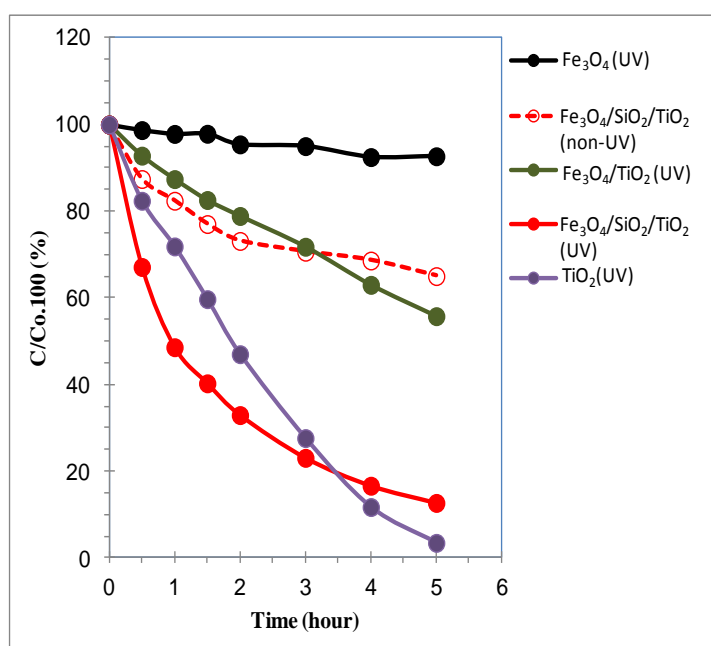


Figure 6 Elimination test of methylene blue under UV irradiation

#### 4. CONCLUSION

The Fe<sub>3</sub>O<sub>4</sub>/SiO<sub>2</sub>/TiO<sub>2</sub> composites have been successfully prepared by the heteroagglomeration method. Two mechanisms have been identified significantly from the Fe<sub>3</sub>O<sub>4</sub>/SiO<sub>2</sub>/TiO<sub>2</sub> composites for methylene blue removal in water, i.e., interacting via the adsorption and photocatalytic processes. The presence of the SiO<sub>2</sub> layer between Fe<sub>3</sub>O<sub>4</sub> and TiO<sub>2</sub> plays a role not only in increasing the efficiency of the photocatalytic activity of TiO<sub>2</sub> but also in serving as the adsorption site in the composites. The resulting Fe<sub>3</sub>O<sub>4</sub>/SiO<sub>2</sub>/TiO<sub>2</sub> composite exhibited an excellent ability to remove dye from water and it is easily collected using a magnetic bar from the photocatalytic slurry reactor.

#### 5. REFERENCES

- Alvarez, P.M., Jaramillo, J., Lopez-Pinero, F., Plucinski, P.K., 2010. Preparation and Characterization of Magnetic TiO<sub>2</sub> Nanoparticles and their Utilization for the Degradation of Emerging Pollutants in Water. *Applied Catalysis B: Environmental*, Volume 100, pp. 338–345
- Bhongsuwan, T., Bhongsuwan, D., Chomchoey, N., Boonchuay, L., 2013. Effect of Calcination Temperature in Production of Magnetic Nanoparticles for Arsenic Adsorption. *In: Paper ID 91 on the 11<sup>th</sup> International Conference on Mining, Materials and Petroleum Engineering, ASEAN Forum on Clean Coal Technology, Chiang Mai, Thailand*
- Calderon, S., Cavaleiro, A., Carvalho, S., 2015. Chemical and Structural Characterization of Zr-C-N-Ag Coatings: XPS, XRD and Raman Spectroscopy. *Applied Surface Science*, Volume 346, pp. 240–247
- Emadi, M., Shams, E., Amini, M.K., 2013. Removal of Zinc from Aqueous Solution by Magnetite Silica Core-shell Nanoparticles. *Journal of Chemistry*, Volume 2013, pp. 1–10
- Fisli, A., Saridewi, R., Dewi, S.H., Gunlazuardi, J., 2013. Preparation and Characterization of Fe<sub>3</sub>O<sub>4</sub>/TiO<sub>2</sub> Composites by Heteroagglomeration. *Advanced Materials Research*, Volume 626, pp. 131–137
- Fisli, A., Yusuf, S., Ridwan, Krisnandi, Y.K., Gunlazuardi, J., 2014. Preparation and Characterization of Magnetite-silica Nano-composite as Adsorbents for Removal of Methylene Blue Dyes from Environmental Water Samples. *Advanced Materials Research*, Volume 896, pp. 525–531
- Hanaor, D.A.H., Chironi, I., Karatchevtseva, I., Triani, G., Sorrell, C., 2012. Single-and Mixed-phase TiO<sub>2</sub> Powders Preparation by Excess-hydrolysis of a Titanium Alkoxide. *Advances in Applied Ceramic*, Volume 111, pp. 149–158
- He, Q., Zhang, Z., Xiong, J., Xiong, Y., Xiao, H., 2008. A Novel Biomaterial-Fe<sub>3</sub>O<sub>4</sub>:TiO<sub>2</sub> Core-shell Nano Particle with Magnetic Performance and High Visible Light Photocatalytic Activity. *Optical Material*, Volume 31, pp. 380–384
- Islam, A.M., Chowdhry, B.Z., Snowden, M.J., 1995. Heteroaggregation in Colloidal Dispersions. *Advances in Colloid and Interface Science*, Volume 62, pp. 109–136
- Jiang, W., Zhang, X., Gong, X., Yan, F., Zhang, Z., 2010. Sonochemical Synthesis and Characterization of Magnetic Separable Fe<sub>3</sub>O<sub>4</sub>-TiO<sub>2</sub> Nanocomposites and their Catalytic Properties. *International Journal Smart and Nano Materials*, Volume 1, pp. 278–287
- Makovec, D., Sajko, M., Selisnik, A., Drogenik, M., 2011. Magnetically Recoverable Photocatalytic Nanocomposite Particles for Water Treatment. *Materials Chemistry and Physics*, Volume 129, pp. 83–89
- Polshettiwar, V., Luque, R., Fihri, A., Zhu, H., Bouhrara, M., Basset, J.M., 2011. Magnetically Recoverable Nanocatalysts. *Chemical Review*, Volume 111, pp. 3036–3075

- Suttiaponparnit, K., Jiang, J., Sahu, M., Suvachittanont, S., Charinpanitkul, T., Biswas, P., 2011. Role of Surface Area, Primary Particle Size, and Crystal Phase on Titanium Dioxide Nanoparticle Dispersion Properties. *Nanoscale Research Letters*, Volume 6(27), pp. 1–8
- Tyrpekl, V., Vejpravova, J.P., Roca, A.G., Murafa, N., Szatmary, L., Nizňanský, D., 2011. Magnetically Separable Photocatalytic Composite  $\gamma$ -Fe<sub>2</sub>O<sub>3</sub>@TiO<sub>2</sub> Synthesized by Heterogeneous Precipitation. *Applied Surface Science*, Volume 257, pp. 4844–4848
- Winataputra, D.S., Dewi, S.H., Wardiyati, S., Fisli, A., 2015. The Photocatalytic Activity of Fe<sub>3</sub>O<sub>4</sub>/SiO<sub>2</sub>/TiO<sub>2</sub> Composite by Mechanochemical Preparation. *Jurnal Sains Materi Indonesia*, Volume 16(2), pp. 54–58
- Wang, R., Wang, X., Xi, X., Hu, R., Jiang, G., 2012. Preparation and Photocatalytic Activity of Magnetic Fe<sub>3</sub>O<sub>4</sub>/SiO<sub>2</sub>/TiO<sub>2</sub> Composites. *Advances in Materials Science and Engineering*, Volume 2012, pp. 1–8
- Zhuravlev, L.T., 2000. Aspects, the Surface Chemistry of Amorphous Silica. Zhuravlev Model. *Colloids and surfaces A: Physicochemical and Engineering Aspects*, Volume 173, pp. 1–38